Nonlinear optical polarization response and plasma generation in noble gases: Comparison of metastable-electronic-state-approach models to experiments

Anand Bahl,[1] Jared K. Wahlstrand,[2,3] Sina Zahedpour,[2] Howard M. Milchberg,[2] and Miroslav Kolesik[1,*]

[1]*College of Optical Sciences, University of Arizona, Tucson, Arizona 85719, USA*

[2]*Institute for Research in Electronics and Applied Physics, University of Maryland, College Park, Maryland 20742, USA*

[3]*Engineering Physics Division, National Institute of Standards and Technology, 100 Bureau Dr., Gaithersburg, Maryland 20899-8443, USA*

The nonlinear polarization response and plasma generation produced by intense optical pulses, modeled by the metastable-electronic-state approach, are verified against space-and-time resolved measurements with single-shot supercontinuum spectral interferometry. This first of a kind theory-experiment comparison is done in the intensity regime typical for optical filamentation, where self-focusing and plasma generation play competing roles. Excellent agreement between the theory and experiment shows that the self-focusing nonlinearity can be approximated by a single resonant state. Moreover, we demonstrate that inclusion of the post-adiabatic corrections, previously tested only in theoretic models, provides a viable description of the ionization rate in real gases.

I. INTRODUCTION

Light is often studied and utilized in situations that require numerical modeling to evaluate and interpret experiments. This is particularly true for ultrafast optics, where simulations of high-intensity, ultrashort optical pulses have been crucial for understanding and control of many phenomena. In this respect, optical filamentation [1–3], or spontaneous hot-spot creation, presents a particular challenge. This is because the light-matter interaction occurs in the specific range of intensities which can be characterized neither as perturbative nor as strong field. At the same time, realistic modeling requires simulations on a scale that precludes efficient description on the quantum level [4–6]. Consequently, phenomenological models have been used, and debates in the literature reflect a level of uncertainty as to what exactly constitutes a proper light-matter interaction model suitable for optical filamentation.

One reason for such uncertainties stems from the lack of truly quantitative comparison between the experiment and theory. Such evaluations are made difficult by the highly dynamic nature of the filament which is extremely hard to quantify experimentally. Difficulties persist also on the modeling side—most models describe the interaction in a piece-wise fashion [7], with parameters often adjusted to a particular wavelength range or even to a given experiment.

This situation is far from satisfactory and motivates the present work. Here we present an extensive quantitative assessment of a computational model against a volume of experimental measurements covering two species of noble-gas atoms over the range of intensities relevant for the femtosecond-pulse dynamics.

Given the difficulties due to evolution in pulses that propagate over significant distances, one can say that the best way to characterize light-matter interaction inside a filament is to avoid the formation of the filament in the first place. This is achieved here by restricting the propagation distance in a thin gas target [8,9]. The nonlinear phase shift in the gas is

measured by single-shot supercontinuum spectral interferometry (SSSI) [10–12]. This pump-probe technique measures the medium nonlinear response resolved in space and time, and through careful optimization of the experimental parameters, propagation effects may be eliminated. This presents an unprecedented opportunity to put numerical modeling through a rigorous test.

The model we test here is the metastable-electronic-state approach (MESA) [13]. This method is sufficiently fast to allow spatially resolved simulation of optical pulses on scales relevant to experiments while, at the same time, drawing from first-principle calculations, it captures both the nonlinear polarization and plasma generation [14]. It is essentially free of adjustable parameters, and was developed and previously tested with the help of time-domain Schrödinger equation (TDSE) simulations. One of our aims here is to refine the value of a sole unknown parameter, previously estimated from TDSE [15], which describes how the ionization yield depends on the excitation wavelength. Our main goal is to verify that the nonlinear light-matter interaction model based on the metastable states is suitable for realistic simulations in nonlinear optics with inert gases.

II. SINGLE-SHOT SUPERCONTINUUM SPECTRAL INTERFEROMETRY

The experimental technique used here is single-shot super-continuum spectral interferometry (SSSI), which measures the space- and time-resolved phase shift $\Delta\Phi(x,t)$ imposed on a probe pulse sampling the interaction of an intense pump pulse with a material medium (see Fig. 1), typically a thin gas target with thickness much smaller than the Rayleigh ranges of the pump or probe. Here, x is a transverse spatial coordinate (to the pump and probe propagation direction) in the medium local to the pump interaction, and defined by the entrance slit of a spectrometer. When coupled with a well-characterized target, absolute measurements of the optical nonlinearity in gases can be performed [9,16]. While nonabsolute transient ionization in gases has been measured using SSSI [17,18],
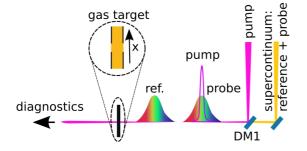
*kolesik@optics.arizona.edu

FIG. 1. Single-shot supercontinuum spectral interferometry. The reference and probe are identical supercontinuum pulses, the latter co-propagating with the pump through the thin gas sample. The reference pulse enters the gas jet first and carries the phase in the absence of the pump. The nonlinear transient phase shift induced by the pump is then obtained by measuring the relative phase between the probe and reference pulses in the frequency domain. Details of the setup are described in Refs. [8–12].

it is much more challenging to do absolute time-resolved measurements, as the highly nonlinear ionization rate requires consideration of the true time resolution of the method [12,17]. The SSSI technique has been described in detail in several earlier publications [8–12]. The experimental setup here is substantially similar, except in the current experiment we extend the capability to measure probe phase shifts $\Delta\Phi(x,y,t)$ in two space dimensions by transversely scanning the probe beam image across the entrance slit.

The pulse envelope is measured with SSSI [11] to be well fit by a Gaussian with the duration (42-fs FWHM). To obtain the peak intensity in the present experiments, we used a CCD camera to record an image of the transverse profile of the pump beam. This image is spatially calibrated, providing the beam shape. The background-subtracted value p of each pixel is related to the (temporal, cycle-averaged) peak intensity by $I_{\mathrm{peak}}(x,y) = Cp(x,y)$. To find the calibration constant C, we use the known n_2^{Ar} of argon [9] and the relation,

$$\Delta\Phi_{\mathrm{peak}}(x,y) = 2kn_2^{\mathrm{Ar}}I(x,y)L_{\mathrm{eff}} = 2kn_2^{\mathrm{Ar}}L_{\mathrm{eff}}Cp(x,y), \quad (1)$$

where $\Delta\Phi_{\mathrm{peak}}(x,y)$ is the peak phase shift, k is the probe wave vector, and L_{eff} is the effective interaction length of the gas target. The calibration constant C is found from the measured $\Delta\Phi_{\mathrm{peak}}(x,y)$ and L_{eff} at intensities below the appearance of ionization. The same C was used to calibrate the data taken in Kr. The total uncertainty in the absolute peak intensity has two sources. The largest source is the uncertainty in the n_2^{Ar} measurement [9], which was 12%. The other source of uncertainty (5%) arises from the fit used to find C. The total absolute uncertainty is thus 13%. However, it is important to note that this reflects the possible error of the overall *scale* of our intensity axis. Because all intensities are referenced to the above number, the relative intensity between data sets is known to considerably better precision (5%) than the absolute intensity.

We will simulate transient nonlinear phase-shift maps numerically, and compare the results against 24 three-dimensional sets of experimental data, for argon and krypton gases.

III. MESA MODEL

The main tool for the numerical simulation utilized in this work is the generalized unidirectional pulse propagation equation [19,20] simulator (gUPPEcore) described elsewhere. Briefly, gUPPEcore is a carrier-resolving, spectral-based simulator in which the treatment of the optical wave-field propagation and its interaction with the medium are compartmentalized, exactly, into separate code components. This allows one to utilize custom-made modules for the description of the light-matter interaction. Here we use an implementation of the metastable-electronic-state approach as described in Ref. [15].

The basic idea of the method is that long-lived (i.e., metastable) resonant electronic states carry a lot of useful physical information [21], and this is despite the fact that such states, also called Stark resonances, do not belong to the Hilbert space assigned to the given quantum-mechanical system [22]. For a long time the resonant energies of various systems have been used to calculate the decay rates given by their imaginary parts. In the optical context, this corresponds to the ionization (e.g., [23–25]) yield when the atom or molecule is exposed to an external electric field, most often realized by a high-intensity optical pulse. Recently, we have shown that in addition to ionization, also the nonlinear response of an atom to the optical field can be captured with the help of such metastable electronic states.

The proof of this concept was first presented in Ref. [13]. For systems of practical importance, we have produced implementations for noble gases [15]. These MESA models are based on applying the single-active electron approximations to inert-gas atoms. In such a framework, the atom is approximated by a single-particle system in which the model electron moves in an effective potential created by the atom nucleus together with the other electrons. It turns out that this approximation is sufficient to obtain the nonlinear indices of inert-gas species which are quite close, given that no fitting parameters were used, to their measured values [14].

The simplest MESA version describes the adiabatic or quasistatic regime, in which the nonlinear polarization P_{NL}, and the ionization rate $\partial_t\rho$, are both slaved to the instantaneous value $F(t)$ of the optical electric field:

$$P_{\mathrm{NL}}(t) = N_a(t)\, e\, a_0\, d_{\mathrm{NL}}(F(t)),$$
$$\partial_t\rho(t) = 2\mathrm{Im}\{E_G(F(t))\}[N_a(t) - \rho(t)], \quad (2)$$

where a_0 is the Bohr radius, ρ is the density of free electrons, and $N_a(t)$ stands for the number density of neutral atoms. Two functions of the field, d_{NL} and E_G, are the nonlinear dipole and imaginary part of the energy of the metastable ground state.

Note that this is only applicable for longer wavelengths when the optical cycle duration is much longer than the atomic time scale set by the atomic potential. This is a quasistatic regime in which the polarization response and ionization rate only depend on the instantaneous value of the field. Small deviations from such a dynamics, termed post-adiabatic corrections here, can be included, albeit approximately, in the MESA model. Post-adiabatic effects should show up both in the polarization response, and ionization yield. The polarization, as a function of time, becomes ever slightly retarded with respect to the driving wave, with a delay given

by a textbook argument based on the ionization potential. This was only recently verified in an experiment [26], showing a delay on the order of a hundred attoseconds. Such a small value is negligible for the present purposes. In contrast, the post-adiabatic effects in the ionization are much more consequential, because they are responsible for the yield dependence on the excitation wavelength. Different methods can be pursued to describe them as a departure from the adiabatic approximation (e.g., [23,27–30]). We have developed an approximation that goes beyond the single-state approach, and which results in a wavelength-dependent correction to the instantaneous ionization rate. The correction can be expressed in terms of the renormalized resonant energy in which the transient shift depends on the rate of change of the electric field $F'(t)$,

$$E_R(t) = E_G(F(t)) + \frac{[F'(t)]^2}{E_{\text{eff}}} \mathcal{M}(F(t),0). \quad (3)$$

Here we have introduced an effective parameter E_{eff}, loosely related to the spectrum of higher-energy resonances, and $\mathcal{M}(F,0)$ is a function that derives from the properties of the ground-state resonance. Together with $d_{\text{NL}}(F)$ and $E_G(F)$, it is tabulated during the one-time characterization of the model atom.

The MESA-based description of wavelength-dependent ionization does not come free, obviously. It is based on several approximations, including the assumption of an off-resonant excitation. We used TDSE simulations to verify that this works in noble-gas atoms exposed to optical pulses, both monochromatic and two-color. The comparison against the numerically exact solutions allowed us to estimate the strength of the post-adiabatic correction to the ionization rate for several species of gases [15]. This reference and its supplemental material provides all tabulated data needed to implement a model as described in Eqs. (2) and (3).

In this work, we verify, through an extensive comparison against SSSI measurements, that MESA not only works, but that its accuracy is sufficient for realistic simulations of many nonlinear-optic scenarios involving noble gases. In these comparisons, we do not adjust any properties that describe the bound-state nonlinear response and/or the ionization rate in the adiabatic regime. It turns out that the properties we have previously obtained from inert gas atom models, using single-active electron approximation, are satisfactory for practical purposes. However, we take this unique opportunity to assess the post-adiabatic correction of the ionization rate, and to refine the sole adjustable parameter present in our model.

IV. EXPERIMENT-THEORY COMPARISON

The following section is devoted to the theory-experiment comparisons. We start with a description of the numerical representation of the SSSI measurement, and continue on with the discussion of results.

A. Simulation of the SSSI experiment

The main output of the SSSI experiment is a three-dimensional space-and-time profile of the probe phase shift $\Phi(x,y,t)$ due to nonlinear interaction of the pump with the
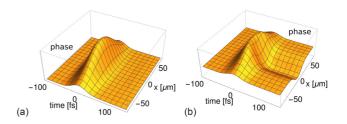

FIG. 2. Typical space-time profiles of the nonlinear phase shift. (a) The Kerr effect dominates at a lower peak intensity, giving rise to a peak that has the same shape as the intensity envelope of the pump pulse. (b) At higher intensity, freed electrons cause depression of the phase shift during and after the pump pulse.

gaseous medium. This is the object that we simulate and compare to the experimental results. The properties of the pump pulse are taken from the experiment. We assume that the pulse is a Gaussian with the duration (42-fs FWHM) and peak intensity as measured.

In the simulation, just as in the experiment, we prepare two identical pulses, the reference and the probe. The reference pulse interacts with the simulated gas jet in the absence of the pump pulse, and thus "records" the reference phase due to propagation through a nonexcited medium. The probe pulse interacts with the gas jet in the presence of the pump, overlapping spatially and temporarily with it just like in the experiment. The phases of the space-and-time resolved complex probe and reference fields are subtracted. This is the nonlinear phase shift detected by the SSSI experiment. This simulation approach produces a phase-shift profile that includes all potential temporal and spatial smearing effects due to propagation through the target (as described in Ref. [10]). Note that it does not include effects caused by, for example, finite spatial and spectral resolution of the imaging system and spectrometer. Such effects are negligible in the experiment for the time and space scales examined here.

Figure 2 illustrates the typical shape of the nonlinear phase shift surface in the space spanned by one transverse coordinate (x) and local pulse time (t). The origin of the coordinate system coincides with the axis of the excitation beam in space and the pulse peak in time.

These illustrative simulation results show that at a low intensity (left panel) one expects to detect a single "Kerr peak," that reflects the local irradiance of the pump pulse. Having measured $\Delta\Phi(x,y,t)$ in this regime gives one access to important parameters of the pump pulse, namely its beam size and the pulse duration.

The right-hand side part of Fig. 2 shows the typical shape of $\Delta\Phi$ in the peak-intensity range that is most relevant to optical filamentation. Here, the pump irradiance is high enough to cause ionization that creates sufficient freed-electron density to counter the phase shift due to the Kerr effect [8]. The plasma signature in this figure is most prominent at later times when the pump pulse intensity is negligible, and the resulting phase shift is simply proportional to the free electron density. This portion of the medium response map provides quantitative information concerning the ionization rate.

An important feature shown in the above figure occurs at a time just after the pump peak. This is when the transient

refractive index change consists of two competing components comparable in strength. This gives rise to a crescent-shaped peak dominated by the Kerr response, but with its central portion modified by the free electrons. In particular, one can see that a depression can evolve where there used to be a peak maximum at lower pulse intensity. In many situations, the dynamics of the propagating pulse coupled to the partially ionized medium inherently gravitates to a regime like this.

Before discussing the results of our simulations, it might be of interest to ask if the experiments in this work could be modeled on a more fundamental level, perhaps employing an integrated Maxwell+Schrödinger solver, such as in Ref. [5]. Given the small interaction volume in our experiments, it should be possible, at least in principle. However, such an undertaking would require an incomparably larger numerical effort. In contrast, the model tested in this work is designed for simulations on scales orders of magnitude larger than what is required for our experiments.

B. Argon

Seventeen experimental data sets were analyzed for argon, with peak intensities of the pump pulse reaching up to $131 \pm 17 \, TW/cm^2$. The peak intensity of each simulation run was set equal to the nominal intensity measured in the experiment. The equivalent propagation length inside of the gas jet was also set to the value(s) measured in the experiment(s), in the range between 400 and $460 \, \mu m$. After the gas jet, linear propagation in vacuum was simulated for a distance between 1000 and $1300 \, \mu m$, depending on the data set, in order to reach the object plane, which was set slightly beyond the gas jet.

There was only a single model parameter that we adjusted by matching a single measured value of the phase shift for one peak intensity. Starting with the value of the post-adiabatic correction obtained previously from a single-active electron model of the argon atom ($E_{eff} = 0.12$), we have adjusted this in order to obtain the measured value of the phase shift for $I_{peak} = 103 \pm 13 \, TW/cm^2$. In particular we targeted the on-axis value at a late time, $\Delta\Phi(x = 0, y = 0, t = 135 \, fs)$, when it is affected solely by the density of free electrons. We obtained $E_{eff} \sim 0.55$, a value which, from Eq. (3), means a weaker correction compared to our previous purely theoretical estimate. We made no adjustments to the other components of the MESA model because, as we shall see next, the agreement between the theory and experiment is rather accurate without further tuning.

First, in Fig. 3 we present examples of the comparison between the experimental and simulated phase shift maps in two-dimensional space, $\Delta\Phi(x, y = 0, t)$. Three different peak intensities (117 ± 15, 95 ± 12, and $42 \pm 5 \, TW/cm^2$) of the pump pulse are selected to demonstrate that the match is excellent across a range of intensities.

In the top portion of the figure, we have $I_{peak} = 117 \pm 15 \, TW/cm^2$. At this high intensity, the plasma generation is so strong that the phase shift due to free electrons becomes significantly larger than that from the Kerr effect. Figures 3(a) and 3(b) show the experimental and simulated color-coded maps of $\Delta\Phi(x, y = 0, t)$, respectively. (In this and in the following figures, the color axis always corresponds to the
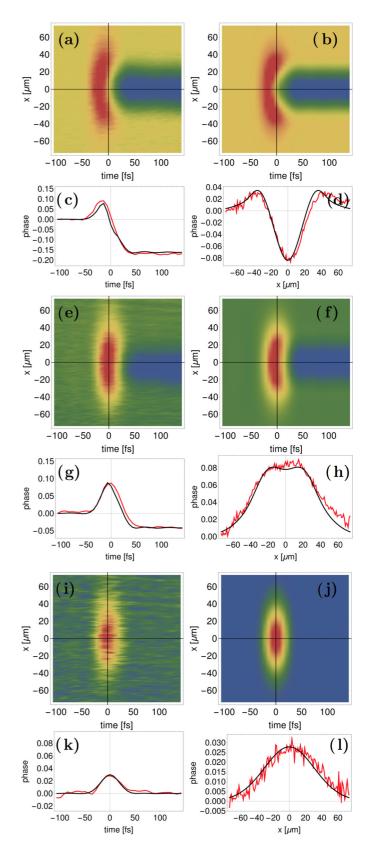

FIG. 3. Space-time resolved, experimental, and simulated phase shifts in argon. Results are shown for three intensities (117 ± 15, 95 ± 12, and $42 \pm 5 \, TW/cm^2$ top to bottom), at which ionization dominates the Kerr effect (top), the two are comparable (middle), and the ionization is small (bottom). The temporal and spatial line-outs follow the lines shown in the space-time plots.
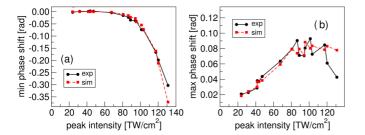
FIG. 4. Measured (black circles) and simulated (red squares) nonlinear phase shifts compared for 17 experimental argon data sets. (a) Maximally negative shifts caused by free electrons in the wake of the excitation pulse. (b) Maximum phase shift, taken over the whole space-time extent. The estimated uncertainty of the horizontal scale due to intensity calibration is about 13%.

range shown in the phase-vs-time plots below.) Here one can clearly see the characteristic shape of the phase-shift surface discussed earlier. In particular, it is evident that at this high intensity, the phase-shift contribution of the free electrons "bites" into the Kerr peak, giving it a pronounced crescent shape with a depressed central value.

For a more detailed comparison, panels below show one-dimensional line-outs at $y = 0$, with the smooth black curve representing the simulation result and the red curve showing the experimental data. Figure 3(c) shows the on-axis temporal profile, $\Delta\Phi(x = 0, t, y = 0)$, while Fig. 3(d) shows the transverse profile $\Delta\Phi(x, t = 0, y = 0)$. Clearly, the agreement is good.

In the middle portion of Fig. 3, [see Figs. 3(e)–3(h)], we show the analogous results for $I_{peak} = 82 \pm 11$ TW/cm^2, for which the peak free electron phase shift is somewhat weaker than the Kerr shift, causing the net phase-shift profile to appear as a flat top. Note that this is the regime the dynamics of optical filamentation tends to reach spontaneously as it seeks a dynamical balance between focusing and de-focusing.

Finally, in the lower part of Fig. 3, in Figs. 3(i)–3(m), we show analogous results for a relatively small peak intensity of $I_{peak} = 35 \pm 5$ TW/cm^2. In this case there is no observed plasma generation. This illustrates that the magnitude of the optical Kerr effect is correctly captured by our model. It may be worthwhile to note that the strength of the Kerr effect here derives solely from the quantum-mechanical calculations of the metastable ground-state properties.

To demonstrate that the good agreement between the theory and experiment is not an accident specific to the three data sets chosen for the above illustration, it is interesting to compile certain characteristics from all 17 experimental sets. This is done in Fig. 4 where we compare maximally negative [shown in Fig. 4(a)] and maximally positive [see Fig. 4(b)] phase shifts $\Delta\Phi$ over the whole measurement or simulation for a given peak intensity of the pump.

The left panel is essentially the signal at late times, when the pump pulse has departed and the phase shift is proportional to the density of free electrons. In other words, the curve shown characterizes the ionization fraction versus peak intensity (of the given pulse). In order to deal with the noise present in the measured data, we have averaged the value of $\Delta\Phi$ over a short time interval. Since the simulated values show no late-

time variations we have used them directly in this and similar figures.

The right-hand-side panel of Fig. 4 shows how the maximal phase shift depends on the intensity. At lower peak intensities, the phase shift increases linearly, as expected for the regime dominated by the Kerr effect. At higher intensities, the curve saturates—this is a sign that the the density of free electrons approaches a range where their de-focusing effect can compete with the self-focusing.

In both panels, the agreement between the measured data and the simulation results is good, although some noise is evident in the experiment (fluctuations in the simulated results originate, most likely, from the gas-jet thickness values of which are taken from the experiment). However, considering the tiny ($\approx 10^{-2}$ radians) nonlinear shifts measured and considering that the modeling is based almost completely on first principles and on the single-state MESA approximation, we find this observation extremely encouraging.

C. Krypton

Seven experimental data sets were analyzed for krypton, with peak intensities of the pump pulse between 31 ± 4 and 105 ± 14 TW/cm^2. Unlike for argon, where the theoretical and measured nonlinear index agree quite closely, in this case there is a small gap between the strength of the Kerr effect as measured in this experiment and as simulated with our single-active-electron MESA model; the simulated self-focusing appears to be weaker than in the experiment. This is why we do not rely on a single experimental set for adjustment of E_{eff}. Rather, we estimated the post-adiabatic correction parameter from the overall agreement across all experimental sets. The previously estimated value of $E_{eff} = 0.11$ [15] had to be raised to $E_{eff} = 0.45$ in order to capture the curve of the ionization yield versus the peak intensity of the pump pulse. Similar to the argon case, this represents a weaker post-adiabatic correction than that obtained from the TDSE simulations in Ref. [15].

Figure 5 shows the comparison of experimental and simulated results for the three peak pump intensities of $I_{peak} = 88 \pm 11$ TW/cm^2 (a)–(d), $I_{peak} = 70 \pm 9$ TW/cm^2 (e)–(h), and $I_{peak} = 26 \pm 3$ TW/cm^2 (i)–(l).

The top portion of Fig. 5 illustrates the regime in which the peak intensity is so high that the de-focusing action of the freed electrons would strongly dominate over the self-focusing effect. Here, even the maximal positive nonlinear phase shift is significantly decreased due to the plasma. In the middle portion, the phase shifts due to the electrons and nonlinear polarization are comparable, and in the lower part of the figure, it is the Kerr effect that is stronger. In this picture, it is evident that the simulated Kerr effect is somewhat weaker than the actual. This is most likely also the reason for the ionization yield being underestimated. Other experimental data sets (not shown) and simulations show the same trends.

Figure 6, a counterpart of Fig. 4, shows a global comparison for all data sets analyzed for krypton. Very much like in the previous case, it demonstrates that there is a good agreement between the experiment and theory for krypton, too. However, the data shown in the right-hand-side panel indicate that the simulated curve is lower than the measured
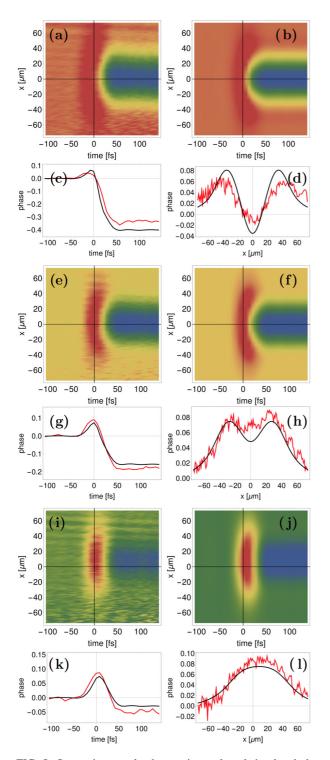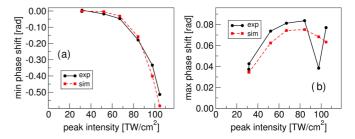
FIG. 6. Measured (circles) and simulated (squares) nonlinear phase shifts compared for seven experimental data sets for krypton. (a) Maximally negative shifts caused by free electrons in the wake of the excitation pulse. (b) Maximum phase shift, taken over the whole space-time extent.

V. DISCUSSION

From the standpoint of the modeling of light-matter interactions in the filamentation regimes, there are two main questions addressed in the present work. First, how do the self-focusing components of the nonlinear response compare between the MESA models and experiments? Second, can the simple description [in Eq. (3)] of the post-adiabatic effects be applied to real atomic gases?

Let us first comment upon the issue of the nonlinear index. We have previously shown that if one extracts the nonlinear index value directly from the nonlinear dipole as a function of the applied field, the resulting n_2 values are reasonably close to their experimental counterparts, but they are consistently lower [14]. We found in the present comparison that this gap is smaller than that expected, especially for argon. This is an encouraging finding which corroborates that the single metastable electronic state can in fact represent the instantaneous optical response. We think that the reason for the model working better in this respect is that the extraction of n_2 from MESA was done [14] at lower intensities than in the present comparison. Of course, MESA never uses any n_2 value, it rather relies on the nonlinear dipole curve $d_{NL}(F)$, and this appears to result in an effective nonlinear index that is higher than the value estimated from its weak-field fit. This is an interesting finding with implications for the interpretation of the instantaneous nonlinearity that we will address in detail in a subsequent work.

Next, let us comment on the issue of the post-adiabatic corrections, and in particular on its strength as represented by parameter E_{eff}. We have taken advantage of the fact that the MESA models for the two inert gases provide a good-enough approximation for the nonlinear polarization in the specific regime explored by the present SSSI experiments. This allowed us to utilize the measured response in order to adjust the value of E_{eff}, while keeping the core of the MESA models (i.e., the functions $d_{NL}(F)$ and $E_{NL}(F)$) unchanged.

We have found that the corrected values, while not too far from those obtained in our previous theoretical study, give rise to weaker post-adiabatic correction (i.e., smaller increase of the ionization yield with decreasing wavelength) than that predicted from the single-active-electron models.

This finding came as a surprise to us, because MESA is designed for longer wavelengths, and the NIR range around 800 nm is at the edge of its applicability. We therefore expected

FIG. 5. Space-time resolved, experimental, and simulated phase shifts in krypton. Results are shown for three intensities ($I_{peak} = 88 \pm 11$ TW/cm^2 (a)–(d), $I_{peak} = 70 \pm 9$ TW/cm^2 (e)–(h), and $I_{peak} = 26 \pm 3$ TW/cm^2 (i)–(l)), at which (top to bottom) ionization dominates the Kerr effect, the two are comparable, and the ionization is small.

one. This indicates that the single-active-electron MESA model underestimates the effective nonlinearity in krypton. Nevertheless, this comparison result validates that the MESA model of krypton is semiquantitatively correct.

stronger, not weaker, corrections at this wavelength. There are several possible reasons why the estimates based on TDSE simulations overestimated the post-adiabatic effects.

First, one has to bear in mind that while single-active-electron approximation may work well to approximate the metastable ground state, it may not be necessarily very accurate for the excited states which could play an increasingly important role at shorter excitation wavelengths.

Second, because the present form of the post-adiabatic correction, as represented by Eq. (3), is a result of several approximations it may be less accurate for $\lambda = 800$ nm.

Third, we must note that our present estimates of E_{eff} are quite sensitive to the calibration of the peak intensity obtained from Eq. (1). In fact, if the calibration is executed with the n_2^{Ar} value only 5% lower, which is well within its experimental error bar, the resulting correction parameters decrease to $E_{\mathrm{eff}} \sim 0.2$. In this sense, even the theoretical estimates are compatible with the experiment, once the uncertainty of the peak intensities is recognized.

The degree of agreement we have obtained with the adjusted values gives us confidence that the post-adiabatic MESA model can approximate real atoms. Moreover, the present results suggest that it is worthwhile to explore further refinements of the dynamics of the post-adiabatic corrections to the ionization rate. More specifically, as a simplest improvement one can consider the evaluation of the renormalized ionization rate according to the memory integral (see [15]) instead of its asymptotic approximation used by the present MESA models. We hope that such improvement becomes feasible when similar measurements as those utilized here become available for mid-infrared wavelengths.

VI. CONCLUSION

This work presents a quantitative comparison between experiments and numerical simulations of ultrashort high inten-sity optical pulses. We have tested a computational model that is based in first-principle physics, but is also capable to support large-scale, fully resolved in time and space simulations of various experiments in nonlinear optics. We have utilized 24 experimental data sets from the single-shot supercontinuum spectral interferometry for two inert gases and a wide range of intensities to verify that the nonlinear spectral shifts predicted by the MESA models agree with those measured.

This comparison stands out in the field of optical filamentation modeling, both in terms of the volume and accuracy of the data involved. This was made possible by SSSI experiments that produce three-dimensional space-and-time resolved maps of the nonlinear phase shifts caused by a strong pump pulse exciting a gas. The accuracy of the SSSI data allowed us to validate the numerically modeled light-matter interaction in the regime that is characterized by simultaneous, competing effects due to bound and free electronic states.

We hope that this work will inspire further quantitative comparisons between experiments and various theories utilized in the field of optical filamentation, but also in the broader context of extreme nonlinear optics.

We trust that the good agreement between our simulations and experiments establishes the metastable-electronic-state approach as a method of choice for simulation of high-intensity optical pulses interacting with noble gases for wavelengths equal or longer than 800 nm.

[1] A. Couairon and A. Mysyrowicz, Phys. Rep. **441**, 47 (2007).

[2] L. Bergé, S. Skupin, R. Nuter, J. Kasparian, and J.-P. Wolf, Rep. Prog. Phys. **70**, 1633 (2007).

[3] S. L. Chin, *Femtosecond Laser Filamentation* (Springer, Berlin, 2009).

[4] E. Lorin, S. Chelkowski, and A. Bandrauk, Comput. Phys. Commun. **177**, 908 (2007).

[5] E. Lorin, S. Chelkowski, E. Zaoui, and A. Bandrauk, Physica D **241**, 1059 (2012).

[6] E. Lorin, M. Lytova, A. Memarian, and A. D. Bandrauk, J. Phys. A: Math. Theor. **48**, 105201 (2015).

[7] A. Couairon, E. Brambilla, T. Corti, D. Majus, O. d. J. Ramírez-Góngora, and M. Kolesik, Eur. Phys. J. Special Topics **199**, 5 (2011).

[8] J. K. Wahlstrand, Y.-H. Cheng, Y.-H. Chen, and H. M. Milchberg, Phys. Rev. Lett. **107**, 103901 (2011).

[9] J. K. Wahlstrand, Y.-H. Cheng, and H. M. Milchberg, Phys. Rev. A **85**, 043820 (2012).

[10] K. Y. Kim, I. Alexeev, and H. M. Milchberg, Appl. Phys. Lett. **81**, 4124 (2002).

[11] S. Zahedpour, J. K. Wahlstrand, and H. M. Milchberg, Opt. Lett. **40**, 5794 (2015).

[12] J. K. Wahlstrand, S. Zahedpour, and H. M. Milchberg, J. Opt. Soc. Am. B **33**, 1476 (2016).

[13] M. Kolesik, J. M. Brown, A. Teleki, P. Jakobsen, J. V. Moloney, and E. M. Wright, Optica **1**, 323 (2014).

[14] A. Bahl, J. M. Brown, E. M. Wright, and M. Kolesik, Opt. Lett. **40**, 4987 (2015).

[15] A. Bahl, E. M. Wright, and M. Kolesik, Phys. Rev. A **94**, 023850 (2016).

[16] J. K. Wahlstrand, S. Zahedpour, Y.-H. Cheng, J. P. Palastro, and H. M. Milchberg, Phys. Rev. A **92**, 063828 (2015).

[17] K. Kim, I. Alexeev, and H. Milchberg, Opt. Express **10**, 1563 (2002).

[18] Y.-H. Chen, S. Varma, I. Alexeev, and H. Milchberg, Opt. Express **15**, 7458 (2007).

[19] M. Kolesik and J. V. Moloney, Phys. Rev. E **70**, 036604 (2004).

[20] J. Andreasen and M. Kolesik, Phys. Rev. E **86**, 036706 (2012).

[21] N. Moiseyev, Phys. Rep. **302**, 212 (1998).

[22] N. Moiseyev, *Non-Hermitian Quantum Mechanics* (Cambridge University Press, Cambridge, 2011).

[23] O. I. Tolstikhin, T. Morishita, and S. Watanabe, Phys. Rev. A **81**, 033415 (2010).

[24] L. Hamonou, T. Morishita, O. I. Tolstikhin, and S. Watanabe, J. Phys.: Conf. Ser. **388**, 032030 (2012).

[25] A. H. Larsen, U. De Giovannini, D. L. Whitenack, A. Wasserman, and A. Rubio, J. Phys. Chem. Lett. **4**, 2734 (2013).

[26] M. T. Hassan, T. T. Luu, A. Moulet, O. Raskazovskaya, P. Zhokhov, M. Garg, N. Karpowicz, A. M. Zheltikov, V. Pervak,

F. Krausz, and E. Goulielmakis, Nature (London) **530**, 66 (2016).

[27] M. Richter, S. Patchkovskii, F. Morales, O. Smirnova, and M. Ivanov, New J. Phys. **15**, 083012 (2013).

[28] G. L. Yudin and M. Y. Ivanov, Phys. Rev. A **64**, 013409 (2001).

[29] M. Hofmann and C. Brée, Phys. Rev. A **92**, 013813 (2015).

[30] J. Doussot, P. Béjot, G. Karras, F. Billard, and O. Faucher, J. Phys. B **48**, 184005 (2015).